Journal of Glaciology

Article

Cite this article: Oien RP, Rea BR, Spagnolo M, Barr ID, Bingham RG (2022). Testing the area–altitude balance ratio (AABR) and accumulation–area ratio (AAR) methods of calculating glacier equilibrium-line altitudes. *Journal of Glaciology* **68**(268), 357–368. https://doi.org/10.1017/jog.2021.100

Received: 5 February 2021
Revised: 12 August 2021
Accepted: 13 August 2021
First published online: 21 September 2021

Keywords:
AABR; AAR; ELA; GIS tool; palaeoclimate

Author for correspondence:
Rachel P. Oien,
E-mail: r.oien@abdn.ac.uk

cambridge.org/jog

Testing the area–altitude balance ratio (AABR) and accumulation–area ratio (AAR) methods of calculating glacier equilibrium-line altitudes

Rachel P. Oien[1], Brice R. Rea[1], Matteo Spagnolo[1], Iestyn D. Barr[2] and Robert G. Bingham[3]

[1]Department of Geography & Environment, University of Aberdeen, School of Geosciences, St. Mary's Building, Elphinstone Road, Aberdeen AB24 3TU, UK; [2]Department of Natural Sciences, Manchester Metropolitan University, Manchester M1 5GD, UK and [3]School of GeoSciences, University of Edinburgh, Drummond Street, Edinburgh EH8 9XP, UK

Abstract

In this study, we compare equilibrium-line altitudes (ELAs) calculated using the area–altitude balance ratio (AABR) and the accumulation–area ratio (AAR) methods, with measured ELAs derived from direct field observations. We utilise a GIS toolbox to calculate the ELA for 64 extant glaciers by applying the AABR and AAR methods to DEMs and polygons of their geometry. The calculated ELAs (c-ELAs) are then compared to measured zero-net balance ELAs (znb-ELAs) obtained from mass-balance time series held by the WGMS for the same glaciers. The correlation between znb-ELAs and AABR (1.56)/AAR (0.58) c-ELAs is very strong, with an $r^2 = 0.99$. The smallest median difference between znb-ELAs and c-ELAs (i.e. 65.5 m) is obtained when a globally representative AABR of 1.56 is used. When applied to palaeoglacier-climate applications, this difference translates to ~0.42°C, well within the uncertainty of palaeotemperature proxies used to determine mean summer temperature at the ELA. The more widely used mean AABR of 1.75 is shown to be statistically invalid due to the skewness of the dataset. On this basis, when calculating glacier ELAs, we recommend the use of a global AABR value of 1.56.

1. Introduction

The glacier equilibrium-line altitude (ELA) is the elevation at which annual accumulation (net gain) and ablation (net loss) are equal. Hence, ELAs can be considered important gauges of climate, reflecting temperature and precipitation at that point on the glacier. More importantly, *changes* to glacier ELAs can be treated as indicators of spatial and temporal response to climate forcing over the instrumental era, as well as providing insights into past climate, and potential responses to future forcing. Time series of ELAs may be analysed to track how glacier mass balance changes from year to year (WGMS, 2017). From these annual data, a climatically representative ELA can be calculated corresponding to the ELA averaged over a standard 30-year window (Sutherland, 1984; Rabatel and others, 2013) or the zero-net balance ELA (znb-ELA) can be calculated as the *y*-intercept value yielded through linear regression of a time series of annual specific net mass balance and ELA, which assumes the glacier is in equilibrium with climate (Rea, 2009).

However, and despite its usefulness, the znb-ELA is rarely calculated, since direct mass-balance data which are notoriously labour-intensive and time-consuming to acquire are currently available for fewer than 150 glaciers globally (Braithwaite, 2008). An alternative approach to making direct ELA measurements is to estimate the ELA using remotely sensed data, including aerial photographs and/or satellite images, by monitoring end of summer season snowlines (as a proxy for the ELA), and/or using multi-annual DEMs to calculate geodetic mass balance. However, in many cases, suitable remotely sensed data (i.e. data with sufficient spatial and temporal resolution, and with limited cloud cover) are unavailable. A further alternative is to calculate the ELAs based on the surface topography/hypsometry of glaciers. The two most widely used techniques for this calculation are the area–altitude balance ratio (AABR) and the accumulation–area ratio (AAR) methods (Carrivick and Brewer, 2004; Rea, 2009; Mernild and others, 2013; Barr and Spagnolo, 2015; Pearce and others, 2017). Both methods generate a calculated ELA (c-ELA), assuming that the glacier is in equilibrium with climate, which is considered comparable to, and a good proxy for, the znb-ELA determined from a measured time series of field surveys (Trenhaile, 1975; Reynaud and others, 1984; Rosqvist and Østrem, 1989; Grudd, 1990; Nesje, 1992; Hagen and others, 2003; Osmaston, 2005). Given that global, relatively high-resolution DEMs are now freely available from several remote-sensing campaigns (e.g. Advanced Spaceborne Thermal Emission and Reflection Radiometer (ASTER); Shuttle Radar Topography Mission (SRTM), Farr and others, 2007; Mathieu and others, 2009), and that multiple glacier outlines have also been digitised and published (from inventories such as GLIMS: Global Land Ice Measurements from Space), the AABR and AAR approaches provide the opportunity to calculate and monitor ELAs for thousands of extant glaciers (Braithwaite and Raper, 2009), even in remote regions where mass-balance records are lacking. This is also key for palaeoglacier studies where

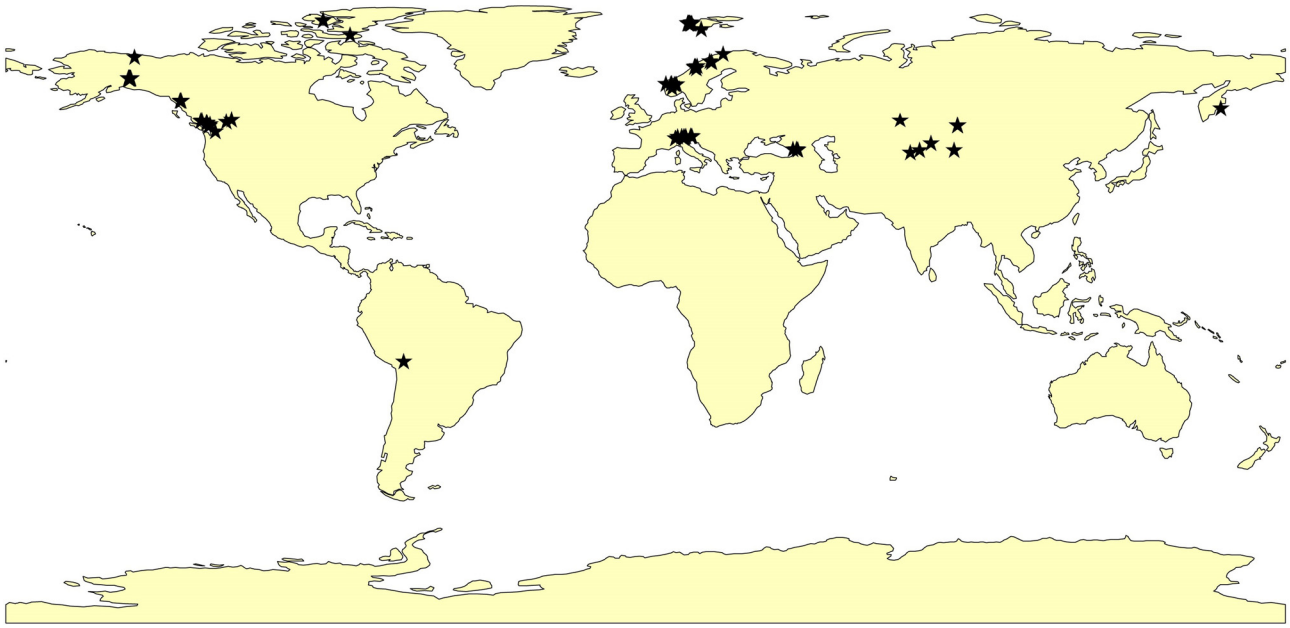

Fig. 1. Distribution and location of the 64 glaciers used within this study which are the same glaciers used in Rea (2009).

numerical (recommended), or cartographic, approaches can be used to generate 3-D reconstructions of palaeoglaciers, from which ELAs can be determined. These palaeo-ELAs are often used to infer palaeoclimate (e.g. Rea and Evans, 2007; Bacon and others, 2001; Barr and others, 2017; Ipsen and others, 2017; Spagnolo and Ribolini, 2019; Rea and others, 2020) using empirical relationships linking ELA, temperature and precipitation (e.g. Ohmura and others, 1992; Ohmura and Boettcher, 2018). When palaeotemperatures are determined from other, independent proxies, reconstructed palaeo-ELAs can be used to generate quantitative estimates of palaeoprecipitation (Benn and Lehmkul, 2000; Mackintosh and others, 2017; Rea and others, 2020), something which is difficult to achieve using other climate proxies.

In all, the hypsometry-based calculation has notable advantages for analysing contemporary and palaeoglaciers. However, the robustness of using both AABR and AAR approaches for ELA calculation has never been systematically tested using a large dataset. To address this shortcoming, here we compare AABR and AAR c-ELAs and measured znb-ELAs (based on empirical field data) for a large, dataset of modern glaciers.

2. Methods

Our assessment is based on 64 glaciers (Fig. 1) for which znb-ELAs are available from Rea (2009). This remains the most comprehensive global inventory of znb-ELAs for which direct, field-measured mass-balance records of ⩾7 continuous years are available between 1999 and 2011 to match the time span of the corresponding ASTER V2.0 and available GLIMS polygons, and hence represents the best available control dataset against which to compare the c-ELAs. For each glacier, Rea (2009) derived the znb-ELA by plotting a time series of annual ELAs against the annual specific net balance, as exemplified in Fig. 2. The original dataset of Rea (2009) comprised of 66 glaciers. However, Kozelskiy and Ram River glaciers were excluded from the original $n = 66$ dataset. Kozelskiy glacier, because there is not a GLIMS polygon for the timeline overlap (GLIMS and NSIDC, 2005, updated 2018). Ram River glacier, because of problems with the outline polygon in GLIMS and the glacier coordinates in the WGMS database. Our final dataset therefore contained 64 glaciers. GLIMS outlines were chosen for this project because they were fit for purpose and the aim was to test free-to-access data. The GLIMS data viewer typically also includes the Randolph Glacier Inventory and the World Glacier Inventory if available (https://www.glims.org/maps/glims).

The aim of the current study is to determine the error between ELAs calculated using open-source datasets (DEMs and glacier outlines) and znb-ELAs determined from measured mass-balance time series. Ideally, we wanted overlapping time windows between the measured mass-balance znb-ELA time series, the DEM acquisition window and the GLIMS mapping year. We defined the best window as 1999–2011, which covers all the GLIMS mapping and ASTER Version 2.0 and most of the WGMS mass-balance time series used by Rea (2009) (Table 1).

To derive c-ELAs for each glacier we used a bespoke ArcGIS toolbox that applies the AABR and AAR methods to DEM data and polygonised glacier outlines (Pellitero and others, 2015). The surface topography of each glacier was extracted from ASTER GDEM Version 2, at 30 m horizontal resolution, freely available through the USGS Earth Explorer (ASTER GDEM Version 2 is a product of METI and NASA, released in October 2011). ASTER V2.0 mean elevation error is between 3.34 and 15.02 m with an average of 8.3 m and a std. dev. of 12.6 m (Tachikawal and others, 2011). Polygons, delineating the perimeter of each glacier, were obtained from the GLIMS global glacier database (Raup and others, 2007; GLIMS and NSIDC, 2005, updated 2018) (Fig. 3; Table 1), and each glacier was labelled using its unique GLIMS code. Google Earth imagery, where possible from the ablation season corresponding to the year of the GLIMS polygon, was used as a cross-check on glacier location and approximate geometry (Fig. 3).

In order to obtain c-ELAs from glacier surface DEMs, appropriate AABR and/or AAR values must be selected. The AABR assumes a fixed ratio between the accumulation and ablation gradients and accounts for the hypsometry of the glacier when calculating the ELA. The AAR more simply assumes the accumulation area occupies a fixed proportion of the total glacier area. Rea (2009) determined global mean values of 1.75 and 0.58 for the AABR and AAR indices respectively, which have been widely adopted by further studies (e.g. Bahr and others, 1998; Kern and László, 2010; Mills and others, 2012; Dong and others,

https://doi.org/10.1017/jog.2021.100 Published online by Cambridge University Press

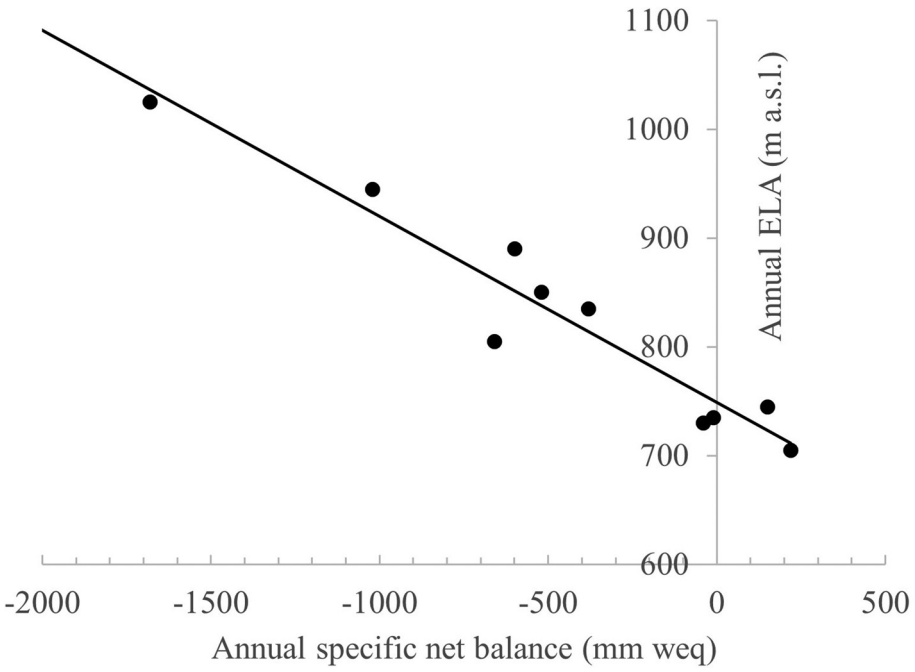

Fig. 2. Plot of annual specific net balance (in mm of water equivalent) vs ELA for Langfjordjøkelen for 10 consecutive years of measurement. The zero-net balance is provided by the *y*-intercept (748 m) i.e. specific net balance is equal to zero.

2017). We applied a skewness test in SPSS® to the AABR and AAR datasets used by Rea (2009), in order to assess if the use of the means was statistically valid. Both datasets failed the test, so global medians were calculated instead, as this statistic better represents skewed distributions. The calculated global median value is 1.56 for the AABR and, fortuitously remained 0.58 for the AAR. We therefore used the median AABR to derive c-ELAs but, for the purposes of comparison with other studies that have used the mean, we also report results generated using the mean global AABR. Braithwaite and Raper (2009) reported a strong correlation between the znb-ELA (their balanced budget ELA) and the median glacier altitude (equivalent to an AAR of 0.5). For completeness, we also determine c-ELAs using an AAR of 0.5 and 0.58 (Table 1).

In addition to considering the global values, c-ELAs were determined using AABR values specific to different regions, also derived from Rea (2009). This analysis was applied to regions here defined as Scandinavia (AABR = 1.5), the North America West Coast (AABR = 2.09), the European Alps (AABR = 1.29) and Central Asia (AABR = 1.75) (Table 2). Again, for completeness we also determined c-ELAs for the Arctic (AABR = 2.91), Eastern Rockies (AABR = 1.11), Kamchatka (AABR = 3.18) and Svalbard (AABR = 2.13) but note that these regional AABRs were derived from only one or two glaciers, so they should be treated with caution. Scandinavia, North America West Coast, European Alps and Central Asia regional datasets passed a skewness test, demonstrating that the mean AABRs calculated by Rea (2009) were valid (Table 2).

It is possible that smaller ice masses, such as cirque glaciers, will have responded more rapidly to ongoing warming than larger ones such as valley or plateau glaciers (Nye, 1965; Grudd, 1990; Bahr and others, 1998) which could affect the comparison between c-ELA and znb-ELA. In order to assess this, we plotted glacial area, taken as a proxy for response time (Raper and Braithwaite, 2009; Zekollari and Huybrechts, 2015; Zekollari and others, 2020), vs the absolute median difference between c-ELA and znb-ELA calculated using the global AABR (1.56). The relationship is statistically insignificant ($r^2 = 0.09$), so it is concluded that differences in glacier response times do not impact the subsequent analyses (see Supplementary data).

3. Results

3.1. c-ELAs vs znb-ELAs for global values

Figures 4a, b, c show the c-ELA determined using the global AABR and AAR values discussed in Section 2. In all instances, the correlation between c-ELA and znb-ELA is very strong ($r^2 = 0.99$). Frequency distributions for the absolute median elevation difference between c-ELA and znb-ELA (Figs 4d, e) show that each dataset is skewed, so the median elevation differences are a more statistically robust metric than the mean. All differences discussed from here onwards will thus refer to the absolute median difference between c-ELA and znb-ELA.

The difference between the c-ELAs and the znb-ELAs for the global median AABR (1.56) is 65.5 m (Table 2) while it is 66.5 m using the global AAR (0.58) (Fig. 4b). The results indicate that the global median AABR produces the smallest median difference between c-ELAs and znb-ELAs, but this is only marginally better than the AAR (0.58). For completeness, we also determined c-ELAs using the AAR value of 0.5 which generated an absolute median elevation difference of 100.5 m. This is worse than those derived using the global AABR (1.56) and AAR (0.58) ratios so the AAR of 0.5 will not be further discussed.

3.2. c-ELAs vs znb-ELAs for the regional AABR values

Figure 5 shows the c-ELAs determined using the regional AABRs for (a) Scandinavia, (b) the North America West Coast, (c) the European Alps and (d) Central Asia. The differences between c-ELAs and znb-ELAs are 51.5, 47, 69.5 and 100 m, respectively. Frequency distributions for the absolute median elevation difference between the c-ELAs and znb-ELAs (Fig. 5e) showed that all the regions followed the same skewness pattern as the global datasets. For Scandinavia, the dataset comprised of 18 glaciers and the c-ELA vs znb-ELAs is again strongly correlated ($r^2 = 0.92$), with an absolute median difference of 51.5 m. This is higher, and therefore less accurate, than the difference of 40.5 m obtained using the global median AABR (1.56) for the same 18 Scandinavian glaciers.

The West Coast Rocky Mountain region contained 13 glaciers and the c-ELAs vs the znb-ELAs are again strongly correlated

https://doi.org/10.1017/jog.2021.100 Published online by Cambridge University Press

Table 1. All the glaciers that are used in the study along with their corresponding WGMS ID, GLIMS code, political unit, latitude and longitude, region (used for regional AABRs), GLIMS SRT-DATE (GLIMS acquisition date of the image used for mapping) and the window of the measured mass-balance time series

Political unit	Region	Name	WGMS_ID	GLIMS_ID	GLIMS_SRT_DATE	Latitude	Longitude	znb-ELA (Rea, 2009) m a.s.l.	c-ELA AABR (1.56) m a.s.l.	c-ELA AABR (1.75) m a.s.l.	c-ELA AAR (0.58) m a.s.l.	c-ELA AABR regional m a.s.l.	c-ELA AAR (0.5) m a.s.l.
BO	Andes	Zongo	1503	G291856E16274S	2000-06-15T00:00:00	−16.28	−68.14	5233	5344	5334	5254	–	5314
CA	Arctic	Devon Ice Cap NW	39	G276838E75498N	1999-06-15T00:00:00	75.42	−83.25	992	1255	1235	1295	2051	1375
CA	Arctic	White	0	G269123E79515N	1999-06-15T00:00:00	79.45	−90.695	901	1181	1095	1015	1091	1341
KG	Central Asia	Abramov	732	G071570E39610N	2002-07-10T00:00:00	39.62	71.56	4159	4187	4228	4207	4228	4247
RU	Central Asia	Djankuat	726	G042766E43192N	2001-09-15T08:19:11	43.1944	42.7612	3193	3273	3263	3283	3251	3281
RU	Central Asia	Garabashi	761	G042470E43302N	2000-09-12T00:00:00	43.3	42.47	3787	3929	3909	3829	3946	3946
KG	Central Asia	Golubin	753	G074498E42454N	2000-08-24T00:00:00	42.46	74.495	3800	3927	3917	3947	3917	3997
RU	Central Asia	Leviy Aktru	794	G087700E50080N	2002-07-10T00:00:00	50.0816	87.6921	3157	3351	3261	3261	3261	3351
RU	Central Asia	Maliy Aktru	795	G087761E50048N	2004-09-10T05:23:25	50.04946	87.74908	3146	3179	3169	3259	3169	3279
RU	Central Asia	Marukhskiy/Marukhi Severniy	727	G041420E43362N	2000-09-12T00:00:00	43.3635	41.4172	2817	2925	2915	2925	2915	2945
RU	Central Asia	Praviy Aktru	831	G087720E50060N	2004-09-10T05:23:25	50.0556	87.7123	3143	3200	3180	3240	3180	3280
KZ	Central Asia	Shumskiy	797	G080229E45083N	2002-07-10T00:00:00	45.08	80.23	3622	3800	3780	3720	3780	3760
KZ	Central Asia	Ts. Tuyuksuyskiy	817	G077081E43044N	2002-07-10T00:00:00	43.05	77.08	3745	3845	3845	3795	3845	3845
CN	Central Asia	Urumqi Glacier No. 1 E-Branch	1511	G086810E43111N	2007-09-13T00:00:00	43.111	86.811	3945	4040	3735	4030	3735	4030
CA	East. Rockies	Peyto	57	G243446E51658N	2006-08-28T00:00:00	51.65991	−116.5638	2619	2633	2623	2653	2653	2683
CA	East. Rockies	Woolsey	1402	G242004E51114N	2006-08-26T00:00:00	51.1141	−118.061	2233	2318	2308	2318	2328	2318
CH	European Alps	Basodino	463	G008475E46414N	2003-08-06T00:00:00	46.42	8.48	2875	2678	2658	2648	2871	2871
IT	European Alps	Careser	635	G010713E46447N	2003-07-30T00:00:00	46.4512	10.7085	3090	3070	3070	3080	3080	2850
CH	European Alps	Gries	359	G008319E46431N	2009-09-15T00:00:00	46.4446	8.3398	2832	2687	2677	2657	2925	2965
AT	European Alps	Hintereisferner	491	G010752E46802N	2003-07-30T00:00:00	46.8	10.77	2921	2889	2879	2929	3089	3119
AT	European Alps	Jamtalfernet	480	G010144E46868N	2003-08-06T00:00:00	47	10.92	2756	2642	2622	2742	2682	2828
AT	European Alps	Kesselwandferner	507	G010788E46845N	2003-07-30T00:00:00	46.8383	10.7933	3107	2948	2938	2998	3180	3210
CH	European Alps	Limmern	421	G008978E46815N	2003-08-06T00:00:00	46.8133	8.9774	2691	2665	2655	2685	2885	2825
AT	European Alps	Ochsentaler Gletscher	483	G010102E46852N	2003-08-06T00:00:00	46.85	10.1	2860	2680	2670	2650	2853	2893
IT	European Alps	Pendente (Vedr.)/ Hangenderf.	675	G011228E46965N	2003-08-24T00:00:00	46.9656	11.2247	2800	2848	2848	2828	2858	2828
CH	European Alps	Silvretta	408	G010084E46850N	2009-09-15T00:00:00	46.85	10.08	2766	2693	2683	2703	2801	2821
AT	European Alps	Vermunt Gletscher	482	G010136E46854N	2003-08-06T00:00:00	46.85	10.13	2800	2675	2665	2675	2805	2825
AT	European Alps	Vernagtferner	489	G010823E46875N	2003-07-30T00:00:00	46.88	10.82	3080	2972	2962	3052	3171	3171
AT	European Alps	Wurtenkees	545	G013004E47039N	1998-06-30T00:00:00	47.0388	13.0054	2887	2867	2867	2697	2953	2953
AT	European Alps	Stubacher Sonnblickkees	573	G012597E47132N	1999-09-07T00:00:00	47.13	12.6	2739	2598	2588	2608	2805	2765
RU	Kamchatka	Koryto	791	G161802E54831N	2000-09-06T00:00:00	54.8307	161.8024	699	815	805	815	765	865
NO	Scandinavia	Engabreen	298	G013853E66657N	1999-09-07T00:00:00	66.65	13.85	1157	1136	1126	1206	1146	1246
NO	Scandinavia	Austdalsbreen	321	G007335E61826N	2006-09-16T00:00:00	61.815	7.352	1427	1485	1485	1515	1495	1535
NO	Scandinavia	Gråsubreen	299	G008600E61657N	2003-08-09T00:00:00	61.657	8.6	2133	2081	2081	2061	2081	2061
NO	Scandinavia	Hansebreen	322	G005672E61746N	2006-09-16T00:00:00	61.75	5.68	1157	1165	1155	1145	1165	1165
NO	Scandinavia	Hardangerjøkulen/ Rembesdalskåka	304	G007405E60537N	2003-08-09T00:00:00	60.53	7.37	1663	1714	1714	1754	1714	1774
NO	Scandinavia	Hellstugubreen	300	G008441E61556N	2003-08-09T00:00:00	61.56	8.44	1837	1868	1868	1898	1878	1918
NO	Scandinavia	Hoegtubreen	286	G013633E66454N	1999-09-07T00:00:00	66.454	13.638	852	978	978	958	978	978
NO	Scandinavia	Langfjordjøkelen	323	G021737E70130N	2006-08-28T00:00:00	70.128	21.735	736	811	801	841	811	901
NO	Scandinavia	Nigardsbreen	290	G007099E61715N	2006-09-16T00:00:00	61.72	7.13	1557	1535	1525	1625	1535	1655
NO	Scandinavia	Okstindbreen	324	G014296E66006N	1999-09-07T00:00:00	66.019	14.294	1310	1265	1255	1305	1265	1345
NO	Scandinavia	Storglombreen	297	G013994E66685N	2002-07-31T09:11:00	66.67	14	1114	1138	1138	1178	1426	1436

NO	Scandinavia	Svartisheibreen	320	G013761E66557N	1999-09-07T00:00:00	66.554	13.762	998	1083	1073	1053	1083	1093
NO	Scandinavia	Trollbergdalsbreen	316	G014437E66716N	1999-09-07T00:00:00	66.716	14.441	1045	1043	1043	1033	1043	1043
NO	Scandinavia	Åalfotbreen	317	G005644E61747N	2006-09-16T00:00:00	61.75	5.65	1201	1201	1191	1211	1201	1221
SE	Scandinavia	Rabots Glaciär	334	G018496E67910N	2002-07-31T09:11:00	67.91	18.5	1368	1474	1464	1454	1474	1484
SE	Scandinavia	Riukojietna	342	G018055E68083N	2002-07-31T09:11:00	68.0836	18.0544	1336	1332	1332	1352	1332	1362
SE	Scandinavia	Storglaciären	332	G018569E67903N	2003-08-09T00:00:00	67.903	18.568	1462	1426	1416	1416	1760	1800
NO	Scandinavia	Storbreen	302	G008261E62524N	2006-01-01T00:00:00	61.57	8.13	1715	1760	1750	1780	1860	1930
NO	Svalbard	Austre Brøggerbreen	292	G011895E78886N	2007-09-01T00:00:00	78.8876	11.8309	281	268	268	278	248	308
NO	Svalbard	Hansbreen	306	G015592E77097N	2008-09-01T00:00:00	77.077	15.63	302	305	295	335	285	355
US	West Coast (NA)	South Cascade	205	G238936E48358N	2003-08-24T00:00:00	48.35029	−121.0554	1885	1880	1870	1850	2805	2765
CA	West Coast (NA)	Alexander	32	G229165E57087N	2005-08-13T00:00:00	57.1	−130.82	1570	1612	1612	1632	1602	1662
CA	West Coast (NA)	Andrei	34	G228969E56957N	2005-08-13T00:00:00	56.93	−130.97	1415	1605	1595	1635	1602	1695
CA	West Coast (NA)	Bench	66	G235089E51445N	2004-07-22T00:00:00	51.43	−124.92	1807	2091	2081	2121	1575	2201
US	West Coast (NA)	Gulkana	90	G214576E63274N	2009-08-04T00:00:00	63.281	−145.427	1732	1752	1732	1762	1778	1898
CA	West Coast (NA)	Helm	45	G237011E49960N	2004-08-09T00:00:00	49.95756	−122.9873	2000	1910	1900	1940	1870	1940
US	West Coast (NA)	McCall	1388	G216152E69302N	2007-08-28T00:00:00	69.3021	−143.8476	1995	2046	2036	2166	2016	2146
CA	West Coast (NA)	Place	41	G237393E50422N	2004-08-09T00:00:00	50.425	−122.601	2081	2119	2109	2059	2099	2089
CA	West Coast (NA)	Sentinel	44	G237020E49886N	2004-08-09T00:00:00	49.886	−122.98	1857	1883	1883	1873	1873	1873
CA	West Coast (NA)	Sykora	59	G236380E50855N	2004-08-09T00:00:00	50.87	−123.58	2156	2233	2223	2253	2203	2303
CA	West Coast (NA)	Tiedemann	24	G234818E51352N	2004-07-22T00:00:00	51.33	−125.05	1658	2131	2111	2071	2071	2181
CA	West Coast (NA)	Yuri	30	G229316E56975N	2005-08-13T00:00:00	56.975	−130.684	1722	1803	1793	1803	1783	1823
CA	West Coast (NA)	Zavisha	46	G236581E50791N	2004-08-09T00:00:00	50.7918	−123.414	2255	2226	2226	2226	2216	2236

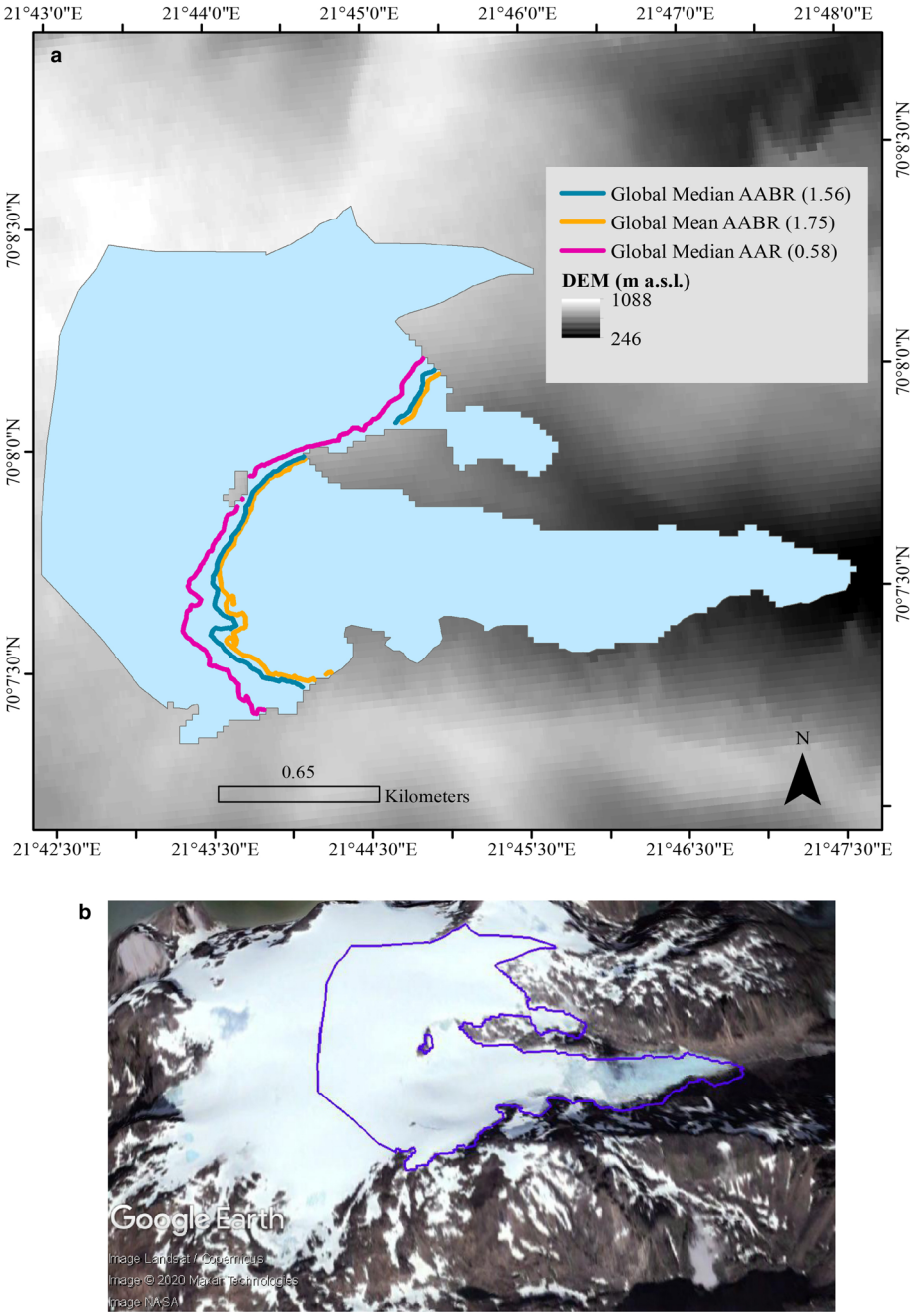

Fig. 3. (a) An example of a glacier polygon from the GLIMS database for Langfjordjøkelen (GLIMS outline acquisition date: 2006). The ELAs presented in this figure were calculated using the GIS tool (Pellitero and others, 2015) described in the methodology using the global AABR and AAR values of Table 2. (b) A snapshot of Langfjordjøkelen (31 December 2006) from Google Earth Pro (Image Landsat/Copernicus) overlain with the corresponding GLIMS polygon.

($r^2 = 0.62$). The absolute median difference is 47 m (Fig. 5b), which is a slight improvement in the result generated using the global median AABR, i.e. 51 m.

For the European Alps, we noted that Vernagtferner had a much higher AABR (2.6) than any of the others in this regional group. A Cook's distance test demonstrates that it is a statistical outlier within the dataset used by Rea (2009) to calculate the regional AABR for the alps. Calculating the regional AABR without Vernagtferner generated a European Alps regional mean AABR of 1.29. c-ELAs for the European Alps dataset of 14 glaciers were then calculated using this new regional AABR. However, this yields only a weak correlation between c-ELA and znb-ELA ($r^2 = 0.33$) with the absolute median elevation difference being 69.5 m. Although large, this elevation difference is lower than the 111 m obtained using the global median AABR.

The Central Asia dataset contained 11 glaciers with the c-ELAs and znb-ELAs having the strongest correlation ($r^2 = 0.94$). Despite this, it has the largest absolute median difference between the two at 100 m which is the same if the global median AABR value is used to determine the c-ELAs.

4. Discussion

4.1. Global indices

The first important result from this study relates to the frequency distribution analyses of the data used by Rea (2009) to generate the global mean AABR (Fig. 4). This has demonstrated that the data are skewed (i.e. not normally distributed), implying that the global mean AABR value of 1.75, calculated by Rea (2009), and widely adopted in many other studies (e.g. Finlayson and others, 2011; Mills and others, 2012; Pellitero and others, 2015; Pellitero and others, 2016; Dong and others, 2017; Pearce and others, 2017; Rea and others, 2020) should not be used. Given the skewness of the frequency distribution, the global median AABR value of 1.56 is instead the statistically valid measure and

https://doi.org/10.1017/jog.2021.100 Published online by Cambridge University Press

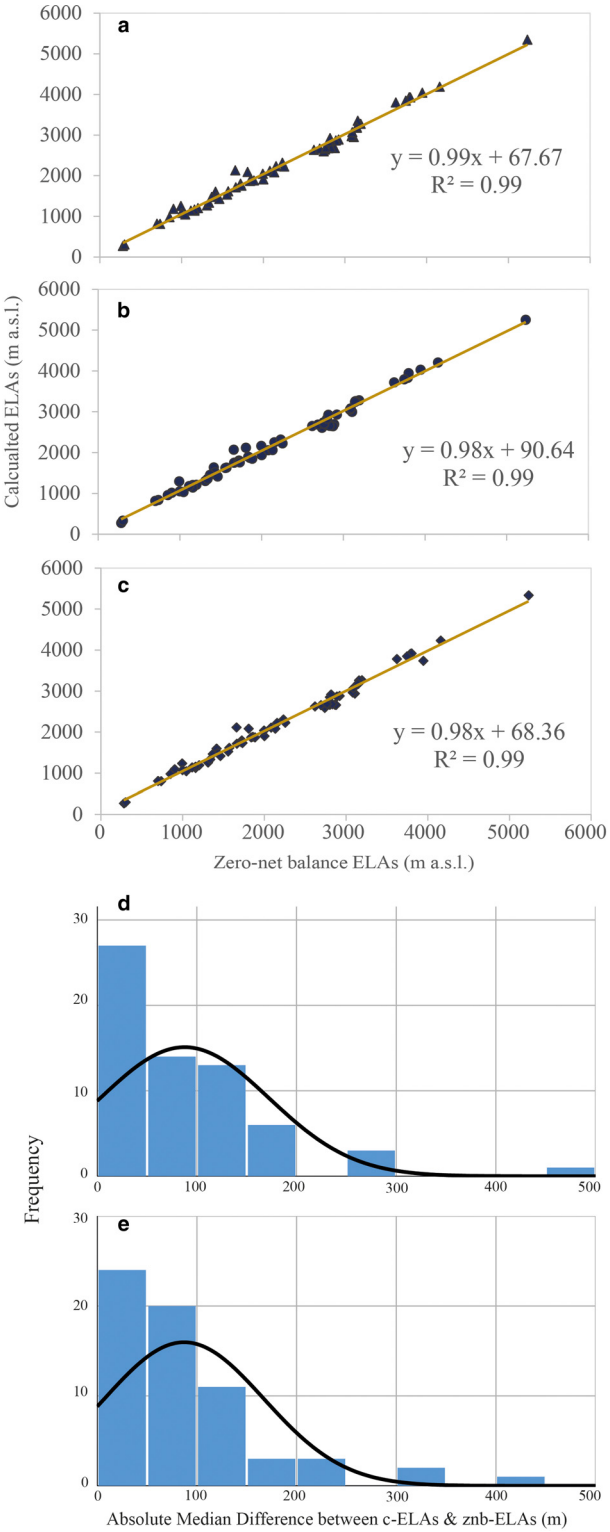

Fig. 4. Comparison of c-ELA and znb-ELA for (a) the global median AABR (1.56), (b) the global AAR (0.58) and (c) the global mean AABR (1.75). In each case, $n = 64$. Histograms of the absolute median difference measurements between c-ELAs and znb-ELAs for each glacier in m, overlain with a normality curve. Note the skewness of the datasets. (d) The normality curve and histogram for the global median AABR (1.56). (e) The normality curve and histogram for the global AAR (0.58).

we recommend this be used for ELA calculation going forward. The global AAR dataset of Rea (2009) is similarly skewed but in this instance the median has the same value as the mean (0.58).

Using the global median AABR, the results show a very strong correlation ($r^2 = 0.99$) between the c-ELAs and znb-ELAs, and hence that there is significant promise for using this method to upscale globally from the limited number of znb-ELA measurements we hold from hard-won annual field surveys. The differences between c-ELA and znb-ELA, calculated using the global median AABR, are not normally distributed about the mean, so we report the absolute median difference between the two as 65.5 m. This is only marginally better than the 66.5 m absolute median difference obtained using the global AAR (Figs 4a, b). These differences can be considered as the potential error associated with calculated glacier ELAs using these methods. Given the availability of open-source, community-built datasets such as GLIMS and ASTER, and the rapidity with which c-ELAs can be determined, this motivates further regional to global-scale ELA assessment to be made wherever elevation data and glacier outlines (or the possibility to retrieve them from remote imagery) are available. Such studies may be used to understand how regional to local climate affects glacier mass balance. Importantly, satellite data provide the opportunity for tracking glacier change in remote and difficult to access regions where direct measurements are lacking and unlikely to be undertaken (Rabatel and others, 2013; Braithwaite and Hughes, 2020). Prior to the satellite era, aerial photographs and topographic maps facilitate the determination of c-ELAs farther back in time (Meier and Post, 1962; Torsnes and others, 1993), thus offering the chance to track glacier response to climate forcing over longer periods, where changes in ELA might be larger than the potential error associated with c-ELAs. Beyond the period of historical records 3-D palaeo-glacier reconstructions allow the calculation of c-ELAs even farther back in time (Kern and László, 2010; Ng and others, 2010; Ipsen and others, 2017) and these are discussed further below.

4.2. Regional AABRs

Although the global median AABR value of 1.56 has been demonstrated to work well in different parts of the world, the use of regional AABR values could represent an improvement in determining ELAs, when sufficient regional mass-balance time series are available (Table 2). For example, in the North America West Coast, the regional mean AABR gives a median difference between the c-ELAs and znb-ELAs of 47 m, which is an improvement in the 51 m difference obtained using the global median AABR. Similarly, using the regional mean AABR for the European Alps results in a decreased difference of 69.5 m between c-ELAs and znb-ELAs, compared to 111 m using the global median AABR. However, 69.5 m remains relatively high and the reason for this is unclear. It is perhaps linked to the small number of znb-ELAs available for the alps ($n = 14$) relative to the diversity in climate along the mountain chain ranging from maritime to continental (Reynaud and others, 1984). With more measured annual ELA time series, there is the potential for determining westeast and perhaps southnorth sub-regional indices. In contrast, in Scandinavia, the difference between c-ELAs and znb-ELAs is 51.5 m, which is larger than the 40.5 m difference obtained using the global median AABR. In Central Asia, the absolute median elevation difference for the regional AABR and global median AABR results in the same outcome of 100 m. Overall, our results indicate that caution should be exercised when choosing the regional over the global AABR.

With increasing monitoring efforts by, for example, the National Institute for Research in Glaciers and Mountain Ecosystems (INAIGEM) in Peru (e.g. Fischer and others, 2016; Nussbaumer and others, 2017) and inventories in the Himalayan region (Bolch and others, 2019) by the Geological Survey of India, Space Application Centre, and Indian Space Research Organization in India (Singh and others, 2016) and others such as ICIMOD (https://www.icimod.org/), the availability of long-term measured glacier mass-balance time series for these currently less represented areas (i.e. Himalaya and Andes) will likely increase. As more data become available for these areas, it will allow for the determination of additional

https://doi.org/10.1017/jog.2021.100 Published online by Cambridge University Press

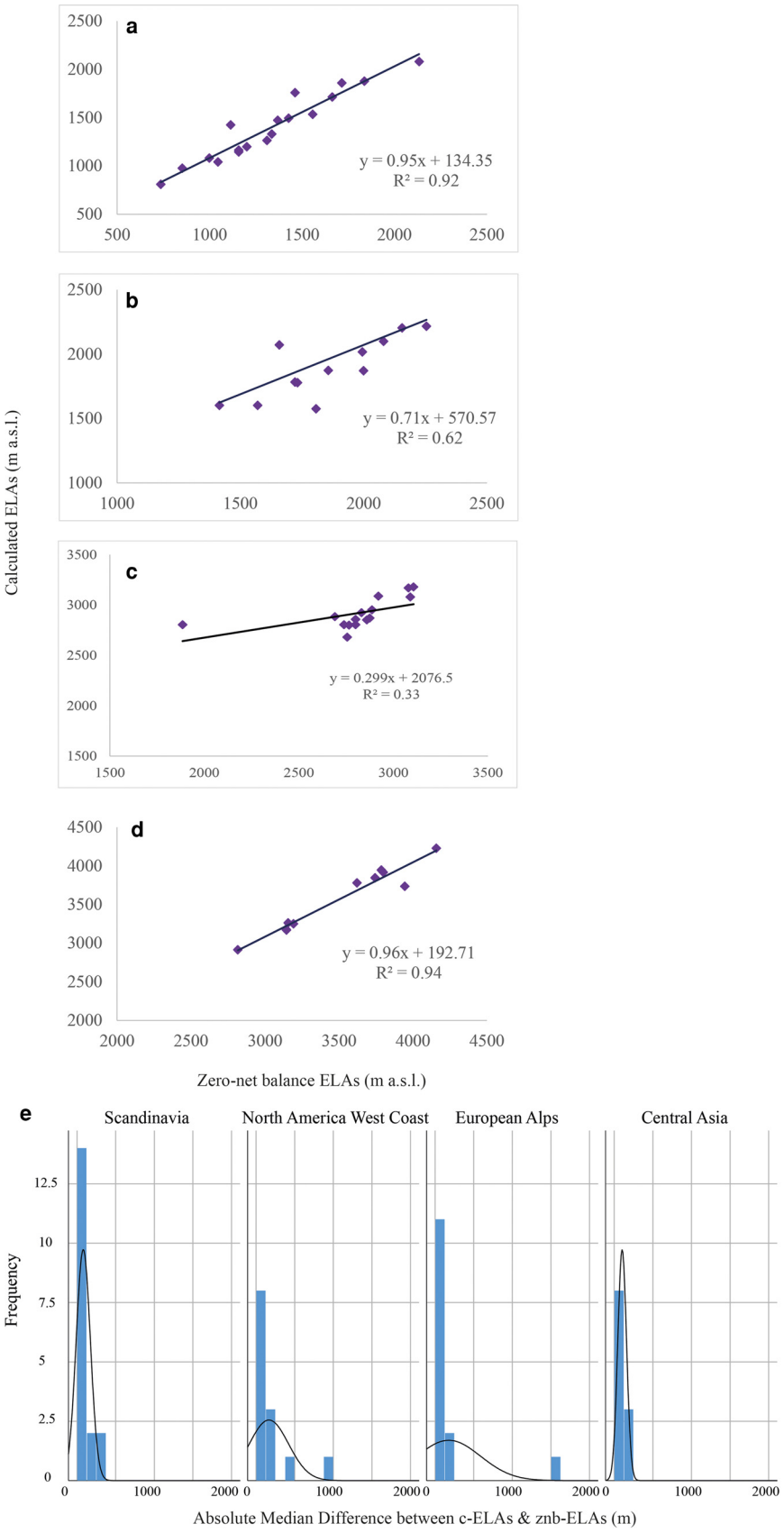

Fig. 5. Cross plot showing the comparison of the c-ELAs versus the znb-ELAs for (a) Scandinavia region using the regional mean AABR of 1.5, $n = 18$, (b) West Coast Rocky Mountain using the regional mean AABR of 2.09, $n = 3$, (c) the European Alps using a new regional mean AABR of 1.29, $n = 14$ and (d) Central Asia using the regional mean AABR of 1.75, $n = 11$. Histograms of the absolute median difference between c-ELAs and znb-ELAs for each glacier in m, overlain with a normality curve. Note the skewness of the datasets. (e) Histograms and normality curves for the three regional AABRs, Scandinavia, North America West Coast, the European Alps and Central Asia.

regional AABR values. Until these become available and are shown to be superior, we recommend the use of the global median AABR of 1.56 for the determination of glacier ELAs everywhere, except for the European Alps and North America West Coast where the use of the respective regional AABR indices provides reduced uncertainty.

4.3. Palaeoclimate applications

c-ELAs have been widely applied in palaeoclimate studies where palaeoglaciers are reconstructed, and palaeo-ELAs calculated (e.g. Pearce and others, 2017). The general procedure is to reconstruct the 3-D surface of the palaeoglacier using an equilibrium

https://doi.org/10.1017/jog.2021.100 Published online by Cambridge University Press

Table 2. Number of glaciers in the dataset, the ratio for each methodology and the difference in the median elevation between the c-ELAs and the measured ELAs using the global median and mean AABRs, the global AAR ratio and the regional AABRs

	Number of glaciers (n)	Ratio	Median elevation difference (1.56/regional AABR) m
Global median AABR	64	1.56	65.5/–
Global mean AABR	64	1.75	66/–
Global AAR	64	0.58	66.5/–
AAR (Braithwaite and Raper, 2009)	64	0.5	100.5/–
Arctic	2*	2.91	271.5/624.5
Central Asia	11	1.75	100/100
Eastern Rockies	2*	1.11	49.5/64.5
European Alps	14	1.29	111/69.5
Kamchatka	1*	3.18	116/66
Scandinavia	18	1.5	40.5/51.5
Svalbard	2*	2.13	8/25
North America West Coast	13	2.09	51/47

Regions noted with * are statistically insignificant but the analyses were undertaken for completeness.

Table 3. Temperature differences (ΔT_{ELA}) resulting from differences between znb-ELAs and c-ELAs when using the global AABR and AAR, and regional AABRs where $n \geqslant 10$

	ΔT_{ELA} °C
Global median AABR (1.56)	0.42
Central Asia (1.75)	0.65
European Alps (1.29)	0.45
Scandinavia (1.5)	0.33
North America West Coast (2.09)	0.31

In each case, a lapse rate of 6.5°C/1000 m is assumed.

profile approach, which requires only evidence for the ice front position, for example a frontal moraine, and the bed topography, obtained from a DEM of the glacier catchment (Pellitero and others, 2016). Other less rigorous approaches have also been utilised, for example, cirque floor altitudes, toe-to-headwall altitude ratio and maximum elevation of lateral moraines (e.g. Miller and others, 1975; Torsnes and others, 1993; Benn and Evans, 2010; Barr and Spagnolo, 2015; Pellitero and others, 2016; Pearce and others, 2017). The reconstructed 3-D surface and the AABR or AAR indices allow the c-ELAs to be easily determined (Pellitero and others, 2015). For the first time it has been demonstrated here that the median absolute difference between c-ELAs, calculated using the median global AABR (1.56), and znb-ELA is 65.5 m and only marginally worse, for the global AAR (0.58) at 66.5 m. For most palaeoglacier–palaeoclimate studies this error is relatively small in comparison with the errors on other proxies required for quantification of palaeoclimate. The ELA of modern glaciers has been linked directly to climate via several empirical relationships, with Ohmura and others (1992) and Ohmura and Boettcher (2018) being the most widely used. In palaeoglacier–palaeoclimate studies if the mean summer air temperature (June, July and August for the Northern Hemisphere) can be determined, for example from chironomidae (Cronin, 1999); Tremblay and others, 2018) or other proxies (Baker, 2009; Farmer and Cook, 2013), these empirical relationships, in combination with the palaeo-c-ELAs, may be used to derive quantitative estimates of palaeoprecipitation. The latter is an extremely useful palaeoclimate parameter and is not well quantified using any other proxies. In addition, palaeoprecipitation may provide information on air mass advection which can be used at a regional scale to reconstruct past atmospheric circulation patterns (Rea and others, 2020). Here, we consider the implications of our findings for such palaeoclimate reconstructions.

Table 4. Effect of the elevation difference between measured and c-ELAs converted to precipitation at the ELA (ΔPP_{ELA}) in mm a^{-1} and as a percentage of total precipitation for the global median and global mean AABRs and global AAR

	Total annual precipitation differences at the ELA		
Mean summer temperatures °C	Global median AABR (1.56) mm a^{-1}, %	Global mean AABR (1.75) mm a^{-1}, %	Global AAR (0.58) mm a^{-1}, %
1	104/8.0	104.8/8.0	105.6/8.1
2	109/7.0	109.8/7.0	110.7/7.1
3	114/6.3	114.9/6.3	115.7/6.3
4	119/5.7	119.9/5.7	120.8/5.8
5	124/5.2	124.9/5.2	125.9/5.3
6	129/4.8	130.0/4.8	131.0/4.9
7	134/4.5	135.0/4.5	136.0/4.5
8	139/4.2	140.0/4.2	141.1/4.2

Precipitation varies as a polynomial function of mean summer temperature (T) so a range of T (1–8°C), representative of alpine environments are provided by way of example.

4.3.1. Uncertainty in palaeotemperature estimation using c-ELAs

In order to assess the implications of the absolute median difference between c-ELAs and znb-ELAs identified above, for palaeoclimate reconstructions, the following approach was applied. The 65.5 m is converted into a temperature difference (ΔT_{ELA}) using a standard lapse rate of 6.5°C per 1000 m, giving a ΔT_{ELA} of 0.42°C (Table 3). When the same methodology is applied to the regional AABR values, for Scandinavia ΔT_{ELA} = 0.33°C, for the North America West Coast ΔT_{ELA} = 0.31°C, for the European Alps ΔT_{ELA} = 0.45°C and for Central Asia ΔT_{ELA} = 0.65°C (Table 3). These levels of uncertainty compare very favourably with those associated with the palaeotemperature proxies used to determine mean summer air temperature at the ELA, which are on the order of ±1.5°C (Rea and others, 2020). It is palaeotemperature that is mostly readily available in most instances which is then used to determine the palaeoprecipitation.

4.3.2. Uncertainty in palaeoprecipitation estimation using c-ELAs

The relationship of Ohmura and others (1992), subsequently Ohmura and Boettcher (2018), is the one most widely utilised to convert palaeotemperature to palaeoprecipitation at the ELA, so this is used to assess the effect of the ΔT_{ELA} identified above. From Ohmura and Boettcher (2018):

$$P = a + bT + cT^2 \quad (1)$$

where at the ELA, T is the mean summer air temperature (J, J, A in the Northern Hemisphere), P is the annual precipitation, a = 966, b = 230 and c = 5.87. As this relationship is a second order polynomial, the implications of ΔT_{ELA} on palaeoprecipitation (ΔPP_{ELA}) will vary, depending on T. Table 4 shows the effect of ΔT_{ELA}, calculated for the uncertainty associated with global AABR and AAR, on ΔPP_{ELA} for a range of T from 1 to 8°C, which is appropriate and representative of many alpine environments. As an example, T = 4°C gives an annual precipitation of 2098.9 mm a^{-1} and±ΔT_{ELA} (±0.42°C for the global AABR), gives an annual precipitation of 2098.9 ± 119 mm a^{-1}, ~±5.7%. For the mean summer temperature range, 1–8°C, the ΔPP_{ELA} ranges between ±104 and 141 mm a^{-1} (±4.2–8.1%) (Table 4). This level of uncertainty is relatively small, and this approach remains one of the few proxies able to quantify palaeoprecipitation.

https://doi.org/10.1017/jog.2021.100 Published online by Cambridge University Press

It has been demonstrated that the regional AABRs for the European Alps and the North America West Coast provide a better estimate for the znb-ELAs but the improvement for Scandinavia is very small (Table 3). Taking the uncertainty of these regional AABR values and a mean summer temperature of 4°C, gives an ΔT_{ELA} and an ΔPP_{ELA} of ±0.33°C and 92.5 mm a^{-1}, ±0.31°C and 85.2 mm a^{-1}, ±0.45°C and 126.3 mm a^{-1} and ±0.65°C and 182.5 mm a^{-1}, respectively, for Scandinavia, the North America West Coast, the European Alps and Central Asia. The decision to use a regional AABR value is more difficult for palaeoglaciers. To do so, makes the implicit assumption that the mass-balance regime in the past was the same as the present-day. It would seem reasonable to use the regional AABRs for Holocene reconstructions unless there was a known and significant difference in the environment relative to the present, for example a contrasting sea ice cover up-wind of the region. Beyond the Holocene, where the boundary conditions relevant to the mass-balance regime are more likely to have been substantially different, it may be more prudent to apply the global median AABR and/or AAR for palaeoglacier-climate studies.

The global mean AABR value of 1.75 reported by Rea (2009) has been widely used in palaeoglacier-climate studies. It has been demonstrated here that the mean is statistically invalid, so the global median AABR of 1.56 should be used for future palaeoglacier ELA calculations. However, Tables 1 and 3 show that using the median AABR makes only a minor improvement in terms of the overall uncertainty, and so is unlikely, in the vast majority of cases, to change the palaeoglacier ELAs calculated previously using the global mean AABR. This will concomitantly make little difference in subsequent palaeoclimate calculations; therefore, authors need not systematically revisit all their previous studies. The only exception to this might relate to glaciers with significantly skewed hypsometry e.g. where a large portion of the accumulation and/or ablation areas lie close to the upper or lower elevation range. In these instances, palaeoglacier ELAs, calculated using the global mean AABR, may alter significantly if the global median AABR (1.56) is used.

5. Conclusions

It has been demonstrated that glacier ELAs, comparable to the znb-ELA determined from a time series of measured annual mass balance, can be calculated for extant glaciers using satellite-derived glacier topography and geometry in combination with AABR and AAR indices. The mean global AABR value of 1.75, reported by Rea (2009) is statistically incorrect, and the global median AABR value of 1.56 should be used instead. ELAs calculated using the global median AABR provides the closest approximation to the measured ELAs (absolute median difference of 65.5 m). In the case of modern glaciers in the European Alps and the North America West Coast, the use of a regional mean AABR reduces the absolute median difference to 69.5 and 47 m respectively (Table 3).

In relation to the two key climate parameters that are linked to the ELA of glaciers, mean summer temperature and annual precipitation (Ohmura and Boettcher, 2018), the absolute median elevation difference between the calculated and the znb-ELAs is relatively insignificant (Tables 3 and 4), and significantly less than, for example, the error on modern gridded climatology (New and others, 1999; Hijmans and others, 2005), which are often used to assess the mass balance of glaciers lacking direct climate measurements (Haylock and others, 2008; Mohr, 2008; Engelhardt and others, 2012).

ELAs of reconstructed palaeoglaciers, determined using the approach outlined above, can be viewed as a robust proxy for palaeoclimate with less uncertainty than many other palaeoclimate proxies. Palaeoglacier ELAs remain one of the few proxies with which to quantify palaeoprecipitation and the errors on those estimates are more dependent on the palaeotemperature proxies. In palaeoglacier-climate research, the application of bespoke ArcGIS toolboxes (Pellitero and others, 2015, 2016) can rapidly yield palaeoglacier reconstructions and palaeoglacier ELAs. In the future for such research, we recommend calculating the ELA using the global median AABR value of 1.56, while cautioning the use of regional AABRs.

Supplementary material. The supplementary material for this article can be found at https://doi.org/10.1017/jog.2021.100

Acknowledgements. The Scottish Alliance for Geoscience Environment and Society (SAGES) and the University of Aberdeen are acknowledged for funding the PhD studentship awarded to Rachel P. Oien. The scientists who have over the years provided data to the WGMS and GLIMS are gratefully acknowledged, as are the USGS and NVE. Additionally, the authors thank Dr Dmitri Mauquoy for assistance regarding the statistical analyses used above. All data used in this publication are publicly available.

Data Availability. ASTER GDEM is a product of METI and NASA (ASTER GDEM Version 2: Accessed July 2019) (https://asterweb.jpl.nasa.gov/gdem.asp). GLIMS and NSIDC (2005, updated 2018): Global Land Ice Measurements from Space glacier database. Compiled and made available by the international GLIMS community and the National Snow and Ice Data Center, Boulder CO, USA. DOI: 10.7265/N5V98602 (http://www.glims.org/MapsAndDocs/ftp.html; https://www.glims.org/maps/glims). Farr, T. G. and others (2007), The Shuttle Radar Topography Mission, *Rev. Geophys*., 45, RG2004, doi:10.1029/2005RG000183 (https://www2.jpl.nasa.gov/srtm/). WGMS (2017): Global Glacier Change Bulletin No. 2 (2014–2015). Zemp, M., Nussbaumer, S.U., Gärtner-Roer, I., Huber, J., Machguth, H., Paul, F. and Hoelzle, M. (eds.), ICSU(WDS)/IUGG(IACS)/UNEP/UNESCO/WMO, World Glacier Monitoring Service, Zurich, Switzerland, 244 pp. Based on database version: doi: 10.5904/wgms-fog-2018-11 (https://wgms.ch/data_databaseversions/). WGMS, and National Snow and Ice Data Center (comps.). 1999, updated 2012. *World Glacier Inventory, Version 1*. [2018]. Boulder, Colorado USA. NSIDC: National Snow and Ice Data Center. doi: https://doi.org/10.7265/N5/NSIDC-WGI-2012-02 (January 2019) (https://nsidc.org/data/G01130/versions/1).

References

Bacon SN and 5 others (2001) Paleo-equilibrium line altitude estimates from late Quaternary glacial features in the Inland Kaikoura Range, South Island, New Zealand. *New Zealand Journal of Geology and Geophysics* **44**(1), 55–67. doi: 10.1080/00288306.2001.9514922

Bahr DB, Pfeffer WT, Sassolas C and Meier MF (1998) Response time of glaciers as a function of size and mass balance: 1. Theory. *Journal of Geophysical Research: Solid Earth* **103**(B5), 9777–9782. doi: 10.1029/98jb00507

Baker PA (2009) Paleo-precipitation indicators. In Gornitz V ed. *Encyclopedian of Earth Science Series: Encyclopedia of Paleoclimatology and Ancient Environments*, Vol. **47**, pp. Dordrecth, The Netherlands: Springer, 746–748. doi: 10.5860/choice.47-2928

Barr ID and 7 others (2017) Climate patterns during former periods of mountain glaciation in Britain and Ireland: inferences from the cirque record. *Palaeogeography, Palaeoclimatology, Palaeoecology* **485**, 466–475. doi: 10.1016/j.palaeo.2017.07.001

Barr ID and Spagnolo M (2015) Glacial cirques as palaeoenvironmental indicators: their potential and limitations. *Earth-Science Reviews* **151**(0), 48–78. doi: 10.1016/j.earscirev.2015.10.004

Benn DI and Evans DJA (2010) *Glaciers and Glaciation*, 2nd Edn. London: Hodder Education. 802 pp

Benn DI and Lehmkuhl F (2000) Mass balance and equilibrium-line altitudes of glaciers in high-mountain environments. *Quaternary International* **2**(65/66), 15–29.

Bolch T and 20 others (2019) Status and change of the cryosphere in the extended Hindu Kush Himalaya region. In Wester P. Mishra A. Mukherji A. and Shrestha A. eds. *The Hindu Kush Himalaya Assessment*, Cham: Springer, 209–255. doi: 10.1007/978-3-319-92288-1_7

Braithwaite RJ (2008) Temperature and precipitation climate at the equilibrium-line altitude of glaciers expressed by the degree-day factor for melting

snow. *Journal of Glaciology* **54**(186), 437–444. doi: 10.3189/002214308785836968

Braithwaite RJ and Hughes PD (2020) Regional geography of glacier mass balance variability over seven decades 1946–2015. *Frontiers in Earth Science* **8**, 302. doi: 10.3389/feart.2020.00302

Braithwaite RJ and Raper SCB (2009) Estimating equilibrium-line altitude (ELA) from glacier inventory data. *Annals of Glaciology* **50**(53), 127–132. doi: 10.3189/172756410790595930

Carrivick JL and Brewer TR (2004) Improving local estimations and regional trends of glacier Equilibrium Line Altitudes. *Geografiska Annaler, Series A: Physical Geography* **86**(1), 67–79. doi: 10.1111/j.0435-3676.2004.00214.x

Cronin TM (1999) *Perspectives in Paleobiology and Earth History*. New York: Columbia University Press, 194–251. doi: 10.1016/0039-6257(79)90170-X

Dong G and 5 others (2017) Cosmogenic 10Be surface exposure dating and glacier reconstruction for the last glacial maximum in the Quemuqu Valley, Western Nyainqentanglha mountains, south Tibet. *Journal of Quaternary Science* **32**(5), 639–652. doi: 10.1002/jqs.2963

Engelhardt M, Schuler TV and Andreassen LM (2012) Evaluation of gridded precipitation for Norway using glacier mass-balance measurements. *Geografiska Annaler, Series A: Physical Geography* **94**(4), 501–509. doi: 10.1111/j.1468-0459.2012.00473.x

Farmer GT and Cook J (2013) Ancient Climates and Proxies. In Climate Change Science: A Modern Synthesis: Volume 1, The Physical Climate, pp. 372–427. doi: 10.1007/978-94-007-5757-8_19

Finlayson A, Golledge N, Bradwell T and Fabel D (2011) Evolution of a late glacial mountain icecap in northern Scotland. *Boreas* **40**(3), 536–554. doi: 10.1111/j.1502-3885.2010.00202.x

Fischer A and 5 others (2016) What future for mountain glaciers? Insights and implications from long-term monitoring in the Austrian Alps. *Developments in Earth Surface Processes* **21**, 325–382. doi: 10.1016/B978-0-444-63787-1.00009-3

Grudd H (1990) Small glaciers as sensitive indicators of climatic fluctuations. *Geografiska Annaler, Series A* **72 A**(1), 119–123.

Hagen JO, Melvold K, Pinglot F and Dowdeswell JA (2003) On the net mass balance of the glaciers and ice caps in Svalbard. *Arctic, Antarctic, and Alpine Research* **35**(2), 264–270. doi: 10.1657/1523-0430(2003)035[0264:OTNMBO]2.0.CO;2

Haylock MR and 5 others (2008) A European daily high-resolution gridded data set of surface temperature and precipitation for 1950–2006. *Journal of Geophysical Research Atmospheres* **113**(20), 1–12. doi: 10.1029/2008JD010201

Hijmans RJ, Cameron SE, Parra JL, Jones PG and Jarvis A (2005) Very high resolution interpolated climate surfaces for global land areas. *International Journal of Climatology* **25**(15), 1965–1978. doi: 10.1002/joc.1276

Ipsen HA, Principato SM, Grube RE and Lee JF (2017) Spatial analysis of cirques from three regions of Iceland: implications for cirque formation and palaeoclimate. *Boreas* **47**(2), 565–576. doi: 10.1111/bor.12295

Kern Z and László P (2010) Size specific steady-state accumulation-area ratio: an improvement for equilibrium-line estimation of small palaeoglaciers. *Quaternary Science Reviews* **29**(19–20), 2781–2787. doi: 10.1016/j.quascirev.2010.06.033

Mackintosh AN, Anderson BM and Pierrehumbert RT (2017) Reconstructing climate from glaciers. *Annual Review of Earth and Planetary Sciences* **45**(1), 649–680. doi: 10.1146/annurev-earth-063016-020643

Mathieu R, Chinn T and Fitzharris B (2009) Detecting the equilibrium-line altitudes of New Zealand glaciers using ASTER satellite images. *New Zealand Journal of Geology and Geophysics* **52**(3), 209–222. doi: 10.1080/00288300909509887

Meier MF and Post AS (1962) Recent variations in mass net budgets of glaciers in western North America. *Proceedings of Obergurgl Symposium* **58**, 63–77.

Mernild SH and 5 others (2013) Identification of snow ablation rate, ELA, AAR and net mass balance using transient snowline variations on two arctic glaciers. *Journal of Glaciology* **59**(216), 649–659. doi: 10.3189/2013JoG12J221

Miller GH, Bradley RS and Andrews JT (1975) The glaciation level and lowest equilibrium line altitude in the high Canadian Arctic: maps and climatic interpretation. *Arctic and Alpine Research* **7**(2), 155. doi: 10.2307/1550318

Mills SC, Grab SW, Rea BR, Carr SJ and Farrow A (2012) Shifting westerlies and precipitation patterns during the late pleistocene in Southern Africa determined using glacier reconstruction and mass balance modelling. *Quaternary Science Reviews* **55**, 145–159. doi: 10.1016/j.quas cirev.2012.08.012

Mohr M (2008). New Routines for Gridding of Temperature and Precipitation Observations for 'seNorge. no.' In Met. no Report (Vol. 8). Retrieved from http://met.no/Forskning/Publikasjoner/Publikasjoner_2008/filestore/NewRoutinesforGriddingofTemperature.pdf.

Nesje A (1992) Topographical effects on the equilibrium line altitude on glaciers. *GeoJournal* **27**(4), 383–391.

New M, Hulme M and Jones P (1999) Representing twentieth-century space-time climate variability. Part I: development of a 1961–90 mean monthly terrestrial climatology. *American Meteorological Society* **12**, 829–856. doi: 10.1175/1520-0442(1999)012<0829:RTCSTC>2.0.CO;2

Ng FSL, Barr ID and Clark CD (2010) Using the surface profiles of modern ice masses to inform palaeo-glacier reconstructions. *Quaternary Science Reviews* **29**(23–24), 3240–3255. doi: 10.1016/j.quascirev.2010.06.045

Nussbaumer SU and 5 others (2017) Glacier monitoring and capacity building: important ingredients for sustainable mountain development. *Mountain and Research Development* **37**(1), 141–152. doi: 10.1659/MRD-JOURNAL-D-15-00038.1

Nye JF (1965) The frequency response of glaciers. *Journal of Glaciology*, 567–587. doi: 10.3189/S002214300001861X

Ohmura A and Boettcher M (2018) Climate on the equilibrium line altitudes of glaciers: theoretical background behind Ahlmann's P/T diagram. *Journal of Glaciology* **64**(245), 489–505. doi: 10.1017/jog.2018.41

Ohmura A, Kasser P and Funk M (1992) Climate at the equilibrium line of glaciers. *Journal of Glaciology* **38**(130), 397–411. doi: 10.3189/S0022143000002276

Osmaston H (2005) Estimates of glacier equilibrium line altitudes by the area × altitude, the Area×Altitude, the Area×Altitude Balance Ratio and the Area×Altitude Balance Index methods and their validation. *Quaternary International* **138–139**, 22–31. doi: 10.1016/j.quaint.2005.02.004

Pearce DM, Ely JC, Barr ID and Boston CM (2017) Section 3.4.9: Glacier Reconstruction. In Geomorphological Techniques (Online Edition). *British Society for Geomorphology* **9**, 1–16.

Pellitero R and 7 others (2015) A GIS tool for automatic calculation of glacier equilibrium-line altitudes. *Computers and Geosciences* **82**, 55–62. doi: 10.1016/j.cageo.2015.05.005

Pellitero R and 9 others (2016). GlaRe, a GIS tool to reconstruct the 3D surface of palaeoglaciers. *Computers and Geosciences*, **94**, 77–85. doi: 10.1016/j.cageo.2016.06.008

Rabatel A, Letréguilly A, Dedieu JP and Eckert N (2013) Changes in glacier equilibrium-line altitude in the western Alps from 1984 to 2010: evaluation by remote sensing and modeling of the morpho-topographic and climate controls. *Cryosphere* **7**(5), 1455–1471. doi: 10.5194/tc-7-1455-2013

Raper SCB and Braithwaite RJ (2009) Glacier volume response time and its links to climate and topography based on a conceptual model of glacier hypsometry. *Cryosphere* **3**(2), 183–194. doi: 10.5194/tc-3-183-2009

Raup B and 5 others (2007) The GLIMS geospatial glacier database: a new tool for studying glacier change. *Global and Planetary Change* **56**(1–2), 101–110. doi: 10.1016/j.gloplacha.2006.07.018

Rea BR (2009) Defining modern day area-altitude balance ratios (AABRs) and their use in glacier-climate reconstructions. *Quaternary Science Reviews* **28**(3–4), 237–248. doi: 10.1016/j.quascirev.2008.10.011

Rea BR and 9 others (2020) Atmospheric circulation over Europe during the Younger Dryas. *Science Advances* **6**(50), 1–14. doi: 10.1126/sciadv.aba4844

Rea BR and Evans DJA (2007) Quantifying climate and glacier mass balance in north Norway during the Younger Dryas. *Palaeogeography, Palaeoclimatology, Palaeoecology* **246**(2–4), 307–330. doi: 10.1016/j.palaeo.2006.10.010

Reynaud L, Vallon M, Martin S and Letreguilly A (1984) Spatio temporal distribution of the glacial mass balance in the Alpine, Scandinavian and Tien Shan areas. *Geografiska Annaler, Series A, Physical Geography* **66 A** (3), 239–247. doi: 10.1080/04353676.1984.11880112

Rosqvist G and Østrem G (1989) The sensitivity of a small icecap to climatic fluctuations. *Geografiska Annaler, Series A: Physical Geography* **71**(1/2), 99–103.

Singh S and 7 others (2016) Changing climate and glacio-hydrology in Indian himalayan region: a review. *Wiley Interdisciplinary Reviews: Climate Change* **7**(3), 393–410. doi: 10.1002/wcc.393

Spagnolo M and Ribolini A (2019) Glacier extent and climate in the Maritime Alps during the Younger Dryas. *Palaeogeography, Palaeoclimatology, Palaeoecology* **536**, 1–11. doi: 10.1016/j.palaeo.2019.109400

Sutherland DG (1984) Modern glacier characteristics as a basis for inferring former climates with particular reference to the Loch Lomond Stadial. *Quaternary Science Reviews* **3**(4), 291–309. doi: 10.1016/0277-3791(84)90010-6

Tachikawal T, Hatol M, Kaku M and Iwasaki A (2011) Characteristics of ASTER GDEM Version 2. *Geoscience and Remote Sensing Symposium (IGARSS), 2011 IEEE International*, 3657–3660. doi: 10.1109/IGARSS.2011.6050017

Torsnes I, Rye N and Nesje A (1993) Arctic and alpine research modern and little ice age equilibrium-line altitudes on outlet valley glaciers from Jostedalsbreen, western Norway: an evaluation of different approaches to their calculation. *Arctic and Alpine Research* **25**(2), 106–116. doi: 10.1080/00040851.1993.12002990

Tremblay MM, Shuster DL, Spagnolo M, Renssen H and Ribolini A (2018) Temperatures recorded by cosmogenic noble gases since the last glacial maximum in Teh Maritime Alps. *Quaternary Research* **91**(2), 829–847. doi: 10.1017/qua.2018.109

Trenhaile AS (1975) Cirque morphometry in the Canadian Cordillera. *Annals of the Association of American Geographers* **66**(4), 517–529.

Zekollari H, Huss M and Farinotti D (2020) On the imbalance and response time of glaciers in the European Alps. *Geophysical Research Letters* **47**, 1–9. doi: 10.1029/2019GL085578

Zekollari H and Huybrechts P (2015) On the climate-geometry imbalance, response time and volume-area scaling of an alpine glacier: insights from a 3-D flow model applied to Vadret da Morteratsch, Switzerland. *Annals of Glaciology* **56**(70), 51–62. doi: 10.3189/2015AoG70A921

https://doi.org/10.1017/jog.2021.100 Published online by Cambridge University Press